IRJSE International Research Journal of Science & Engineering
Int. Res. J. of Science & Engineering, Special Issue A12, February, 2023 SJIF Impact Factor 6.70
ISSN: 2322-0015 https://doi.org/10.5281/zenodo.7763091
RESEARCH ARTICLE **OPEN ACCESS**

Modified Structural, Optical and Electrochemical Properties of Nickel Sulphide for Superior Supercapacitor Electrode

Pratik Patil†, Khushalchand Garud†, Rohini Burungale, Kajal Sawant, Divya Salunkhe, Prajakta Gavade, Shubhangi Bhosale, Swapnil Rajoba, Vijay Mohite, Pandurang Pingale, Rajendra Kale, Sachin Kulkarni*

Advanced Electrochemical Laboratory, Department of Physics, Tuljaram Chaturchand College of Arts, Science and Commerce, Baramati, 413102, (MH) India.
Email:sachinbkul@gmail.com

Manuscript Details
Available online on https://www.irjse.in
ISSN: 2322-0015

Editor: Dr. Arvind Chavhan

Cite this article as:
Pratik Patil, Khushalchand Garud†, Rohini Burungale, Kajal Sawant, Divya Salunkhe, Prajakta Gavade, Shubhangi Bhosale, Swapnil Rajoba, Vijay Mohite, Pandurang Pingale, Rajendra Kale, Sachin Kulkarni. Modified Structural, Optical and Electrochemical Properties of Nickel Sulphide for Superior Supercapacitor Electrode, *Int. Res. Journal of Science & Engineering,* 2023, Special Issue A12: 1-10. https://doi.org/10.5281/zenodo.7763091

Article published in Special issue of International Conference on "Recent Trends in Materials Science, Synthesis, Characterization and Applications (RTMS-2023)" organized by Department of Physics, Anekant Education Society's, Tuljaram Chaturchand College of Arts, Science and Commerce, Baramati, Dist Pune, Maharashtra, India (Autonomous) date, January 3-4, 2023.

Abstract

Nickel sulphide is one of the proficient electrode materials for supercapacitors. Current abstract portrays about thin film deposition of nickel sulphide by simple chemical route and further improvement in structural, morphological, optical and electrochemical properties is obtained by heat treatment.

Comparative analysis of as-deposited and annealed nickel sulphide thin film electrodes is characterized via XRD, FESEM, UV and electrochemical testing. X-ray diffraction shows amorphous to polycrystalline transformation and renders flakes like morphology for both as deposited and annealed samples. Moreover, optical band gap decreases after annealing from 2.67 to 2.36 eV reveals, red shift as well as improved in crystallinity of sample. This ritual effect results in boosting of electrochemical performance of nickel sulphide electrode by lowering impedance i.e. charge transfer resistance. Thus, annealing process offers more accessible electrode-electrolyte interaction towards flake like morphology and causes increase in capacitance. Nickle sulphide electrode shows specific capacitance value of 655 Fg^{-1} at 10 mVs^{-1} scan rate and 641 Fg^{-1} at 1.0 mAg^{-1} current density in 1M KOH aqueous electrolyte with ~83% stability for 1000 cycles. Hence, improvement in the structural, optical, and electrochemical properties and performance for nickel sulphide electrode is suitably attained and employed for supercapacitor application by Simple chemical method.

Keywords: Nickel sulphide, modified Properties, Supercapacitor, Electrode, Simple chemical method

Graphical Abstract:

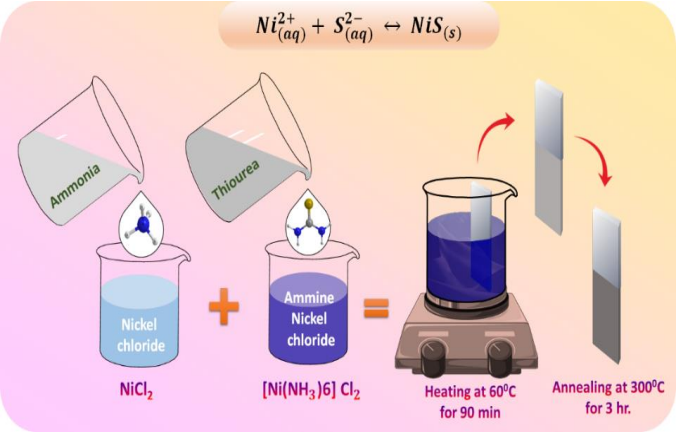

Schematic: Formation of flakes like NiS thin film by simple Chemical bath method.

Introduction

The most significant issues in electrochemical technology are usually new renewable energy sources and energy storage materials [1]. In recent years, the increased demand for electrical vehicles, portable devices, and other electronic devices that require excellent electrical energy at eminent power levels in electrochemical supercapacitors due to their outstanding characteristics of long cycling life, high power density, rapid recharge capability, higher capacitance, light weight, and flexibility [2-4]. Transition metal sulphides, such as cobalt sulphide (CoS), nickel sulphide (NiS), molybdenum sulphide (MoS), copper sulphide (CuS), and others, have recently been identified as a promising class of active electrode materials due to their reasonably high specific capacitance values and exceptional redox reversible reaction activities [5,6]. Among them, NiS is a viable choice for Supercapacitor applications because it has many positive properties such as high theoretical specific capacity, low cost, simplicity of production, low toxicity, and environmental friendliness [7]. It can exist in different thermodynamically stable crystal structures and stoichiometric forms such as NiS, NiS_2, Ni_7S_6, Ni_6S_5, Ni_9S_8, Ni_3S_2 and Ni_3S_4 each having different catalytic activity which depending on the structure and morphology [8] Nowadays, nickel sulphides with different morphologies have been synthesized through various methods, such as physical vapor deposition, chemical vapor deposition, electrochemical deposition, chemical bath deposition (CBD), hydrothermal and solution growth techniques, etc. [9] These methods often require high growth temperature and structure directing agents in addition to toxic organic solvents.

Zhu, *et al.* [10] prepared CNT@Ni_3S_2 nanosheets electrode achieved a specific capacitance of 586 Fg^{-1} at 1 mVs^{-1}, Yang *et al.* [11] synthesized flower-like β-NiS via solvothermal method that achieved a specific capacitance of 512.96 Fg^{-1} at 5 Ag^{-1}. Patil *et al.* [12] synthesized flower-like β-NiS via hydrothermal process showed a specific capacitance of 415.78 Fg^{-1} at 0.5 $mAcm^{-2}$ current density. Nandhini *et al.* [13] showed specific capacitance 482 Fg^{-1} at 10 mVs^{-1} of NiS nanostructures via microwave assisted hydrothermal method. Interconnected NiS synthesized by Yu *et al.* [14] using simple soaking method on Nickel foam showed specific capacitance of 484 Fg^{-1} at 5 $mAcm^{-2}$**.** Previous research revealed that annealing can improve structural, optical, and electrochemical activity of metal sulphides. An electrode developed in this manner can achieve high specific capacitance values than the pristine electrodes. further CBD is one of the most advanced and straightforward nanostructure deposition techniques used for thin films deposition which providing Large adherent film with a low operating cost, this methodology also definitely contributes to increase specific capacitance [15,16].

In this study, we demonstrate the preparation of NiS on stainless steel (SS) substrate by simple, low-cost Chemical bath method (CBD). This methodology is a more efficient, energy saving and convenient route to form a stable structure and effective morphologies of NiS electrodes. Furthermore, the experimental conditions may be changed to influence the structural, morphological, and electrocatalytic properties of the deposited material. NiS was deposited from the aqueous solution of Ni and S precursors with the addition of complexing agent. The as-prepared samples were annealed at 300°C to get polycrystalline NiS. Annealing can improve structural, optical, and electrochemical properties of NiS. The prepared

samples were examined by various physicochemical characterization to investigate its crystallinity and morphological) techniques and charge discharge stability.

Methodology

Material preparation:

All chemicals were of analytical grade (A.R) without further refinement. Nickel dichloride (Hexahydrate) extra pure [$NiCl_2 \cdot 6H_2O$], Thiourea 99% AR [CH_4N_2S], and Ammonia Solution 30% AR/ACS [NH_4OH]. NiS films were obtained from an aqueous solution of double distilled water. The glass substrates were cleaned with labolene detergent, thoroughly washed with double distilled water (DDW) and further subjected to chromic acid treatment. Finally, these substrates were sonicated in water bath for 10 min. The films on glass substrate were used for optical studies and the Stainless-Steel Substrate (4×1 cm^2) was used for structural, morphological and electrochemical studies. Before use SS substrates were well polished with zero-grade polish paper.

Synthesis of NiS thin film electrode:

Synthesis of NiS thin films electrode by lucrative CBD is based on the immersing the substrates into a Nickel chloride aqueous bath complexed with ammonia solution. The reaction bath including 0.05 M Nickel dichloride hexahydrate ($NiCl_2 \cdot 6H_2O$) as source of Ni^{2+} metal was dissolved in 25 ml double distilled water (DDW) by continuous magnetic stirring. This cationic precursor was complexed with 30 ml ammonia solution. The ammonia controlling the rate of reaction through regulate pH value. The solution resulted into transparent homogeneous blue coloured solution. Further anionic precursor, 0.2 M thiourea separately prepared in 25 ml DDW as source of Sulfur. This anionic precursor was continuously added to the well complexed cationic precursor and stirred well for 5 min. The pH of the resultant bath solution was 11.5. The glass and stainless-steel substrates were immersed in the bath placed at 60°C. When the bath attained the temperature of 60°C, the precipitation (homogeneous blue in colour) started in the bath. During the precipitation, heterogeneous reaction occurred and deposition of hydrous NiS took place on the substrate surface. Further, thermal treatment resulted into formation of polycrystalline NiS electrode.

Materials characterization:

The X-ray diffractometer (CuKα target) were used to identify the structural properties of NiS films. A Shimadzu UV-1800 UV/Visible Scanning Spectrophotometer was used to evaluate the optical absorption of NiS thin film on glass substrate within wavelength range 300-800 nm. Microstructure of films was studied using Field Emission Scanning Electron Microscopy (FE-SEM, Mira-3, Tescan Pvt.). The electrochemical analysis of the NiS films deposited on steel substrate was studied by CV using the Potentiostat (ZIVE MP1, Electrochemical Potentiostat). The three-electrode cell setup was equipped for testing supercapacitor studies. The electrochemical cell consists of platinum sheet as a counter electrode, saturated calomel electrode (SCE) as a reference electrode, and annealed NiS thin sheet as a working electrode in 1 M KOH electrolyte. The influence of scan rate and current density variation on specific capacitance was investigated.

Result and Discussion

1. **Film formation mechanism:**

When the solution is saturated in the chemical deposition process, film formation is observed. Precipitation occurs when the ionic product of anion and cation exceeds the solubility product of metal oxide, and ions combine on the substrate in the solution to form nuclei [17]. Film formation can occur by ion-by-ion condensation from solution on to substrate. Nucleation and particle growth are two crucial processes in the formation of solid phases from solutions. The rapid separation of molecular clusters formed during nucleation, causes substrate particle aggregation [18].

In deposition of NiS thin film, cation and anion precursors were prepared separately before combining. In the first stage for cation precursor, nickel chloride is complexed by ammonia solution. After the addition of

ammonia solution, Ni^{2+} ions get complexed with ammonium ion. Stoichiometrically, the output in the form of ammine nickel chloride can be represented in cation complexation reaction (1).

$$NiCl_2 .6H_2O + 6NH_4OH \rightarrow [Ni(NH_3)_6]Cl_2 + 12H_2O \quad (1)$$

Further, anion precursor thiourea is added into the above solution with continuous stirring and final bath is subjected to 60°C for 90 min. This thermal kinetics breaks metal complexes and make available Ni^{2+} ions to react with S^{2-} ions of thiourea in controlled manner for the formation of NiS thin film. This leads to formation of NiS flakes with porous structure on the surface of SS substrate as represented in equation (2).

$$Ni^{2+}_{(aq)} + S^{2-}_{(aq)} \xrightarrow{\Delta} NiS \downarrow \quad (2)$$

The hydrous NiS sample is subjected for heat treatment and was annealed at 300°C for 3hr. Finally dark blackish coloured adherent NiS thin film is appeared. Further as deposited and anneled samples are subjected for characterizations.

2. Structural studies:

The XRD patterns were recorded in the 2 θ range 10-80° to investigate the crystalline nature of the as-prepared and annealed thin films. The XRD patterns of as prepared and annealed thin film on stainless steel substrate are shown in Fig 1. This revealed that, as deposited electrode showed amorphous NiS while annealed sample is with improved crystallinity.

The annealed electrode showed the diffraction peaks at 2θ= 29.33°, 34.21° and 60.12° are attributed to the hkl plane (100), (101) and (103) respectively. These peaks are corresponding to hexagonal structured NiS (JCPDS ref no. 01-077-1624). Similar diffraction data has been observed by Pan, Y *et al.* [19]. Some common sharp intense peaks appeared in both patterns of as deposited and annealed samples at angles ~43°, ~44°, ~51° and ~75° are assigned to SS substrate. However, other impurity is not observed in the NiS thin films prepared at 300°C annealed temperature. The lattice parameters a, b, and c for hexagonal phase was determined by using the following equation 3.

$$\frac{1}{d^2} = \frac{4}{3}\left(\frac{h^2+hk+k^2}{a^2}\right) + \frac{l^2}{c^2} \quad (3)$$

For hexagonal lattice, $a = b \neq c$, in the above relation, h, k and l are miller indices of reflector planes appearing on the diffraction spectrum and d is their interplanar distance [20]. The obtained average lattice constants were found to be a = 3.4390 Å, b = 3.4390 Å, and c = 5.3240 Å. These values are consistent with standard JCPDS reference data. The average crystallite size (D) of the prepared films was calculated by the Scherrer formulation [21],

$$D = \frac{k\lambda}{\beta \cos\theta} \quad (4)$$

where k is the constant term with value k = 0.94, λ is wavelength of x-ray (λ= 1.5406 Å), β is the full width at half maxima of diffraction peak, and θ is the Bragg's angle. The average crystallite size of the annealed NiS sample was 39.73 nm. The interplanar d-spacing were calculated by the following formulation [22],

$$2dsin\,\theta = n\lambda \quad (5)$$

where d is the interplanar d-spacing, θ is the Bragg's angle, n is the order of diffraction (usually n = 1), and λ is the wavelength of the x-ray used (here, λ = 1.5406 Å). All the values of d-spacing corresponding to diffraction peaks are tabulated in table. Micro strains occur in the films because of the stresses. The micro strains are calculated by the following formula [23]

$$\varepsilon = \beta cos\theta / 4 \quad (6)$$

The micro strains of the annealed NiS sample was 0.0012. Internal micro strain can readily lead to the creation of defect. The dislocation density (δ) values can be obtained by following formulation and observed to be 0.0006 lines.m^{-2} [24],

$$\delta = 1/D^2 \quad (7)$$

The values of microstructural factors like interplanar d-spacing [Å], Crystalline size (D), Dislocation density (δ) and micro strain are charted in table. The deformation like dislocation and micro strain has Influence on energy storage capability in materials. All the values related with the microstructural analysis of annealed NiS electrode indicates that the electrode has ability to store large amount of energy.

Table1. X-ray diffraction data for Crystalline size, Dislocation Density, Micro- strain, and band gap) of the annealed NiS electrode.

2 θ	(hkl)	d-spacing [Å]	Crystalline size (D) (nm)	Dislocation Density (δ) (Lines.m^{-2})	Micro- strain (ε) × 10^{-3}	Band gap (eV)
29.33	(100)	2.9782	39.73	0.0006	1.2	2.36
34.21	(101)	2.5992				
60.12	(103)	1.52453				

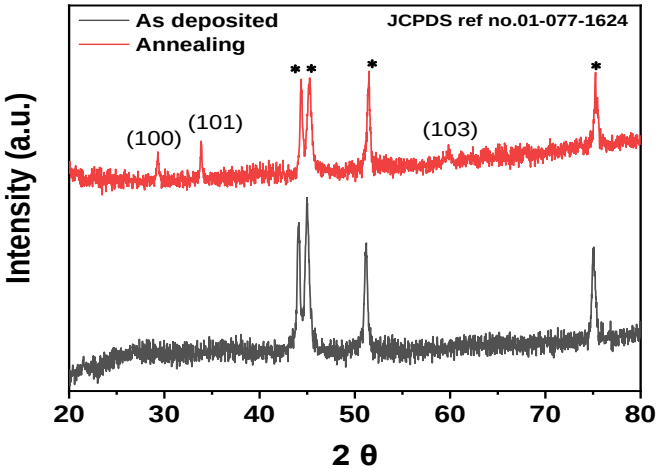

Fig. 1. The XRD patterns of as deposited and annealed NiS thin film on SS substrate

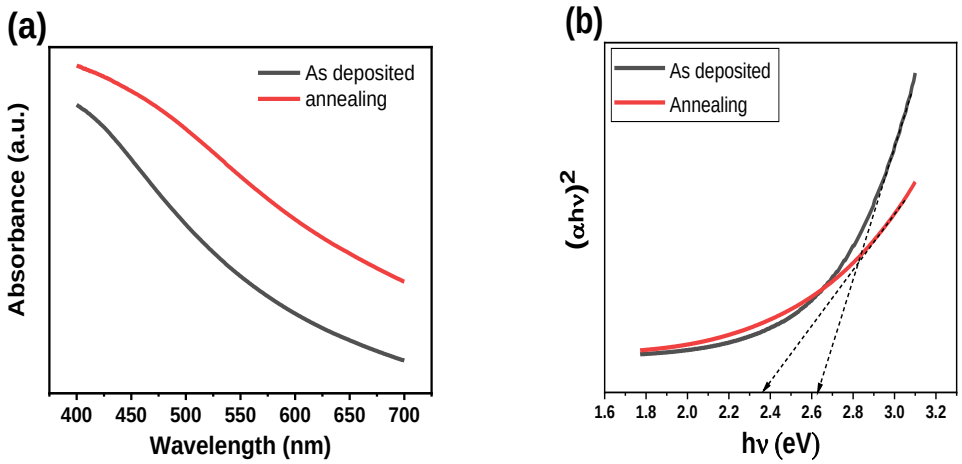

Fig. 2. (a) absorption spectra (b) band gap for as deposited and annealed NiS thin films.

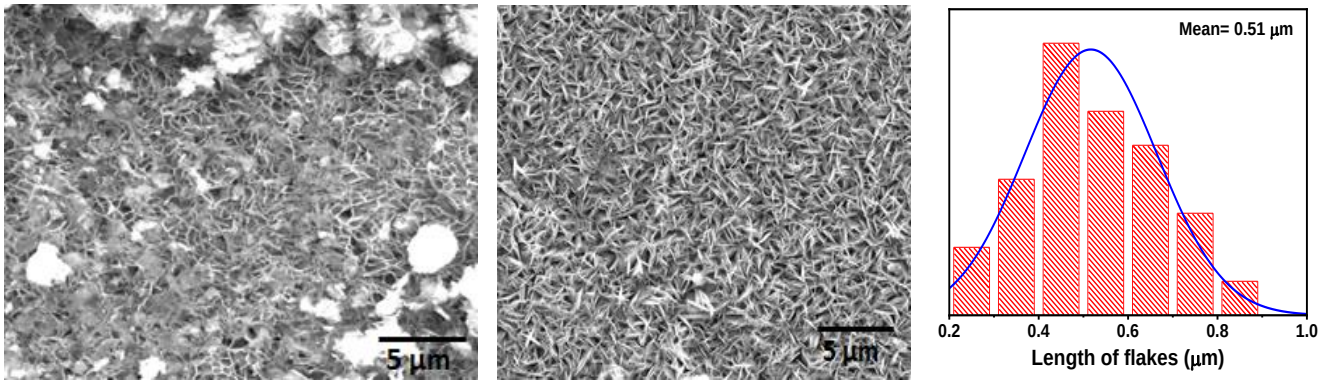

Fig. 3. FE-SEM image of NiS thin film at magnifications of 5 µm. (a) as deposited (b) Annealed and (c) Histogram indicates average length of flakes.

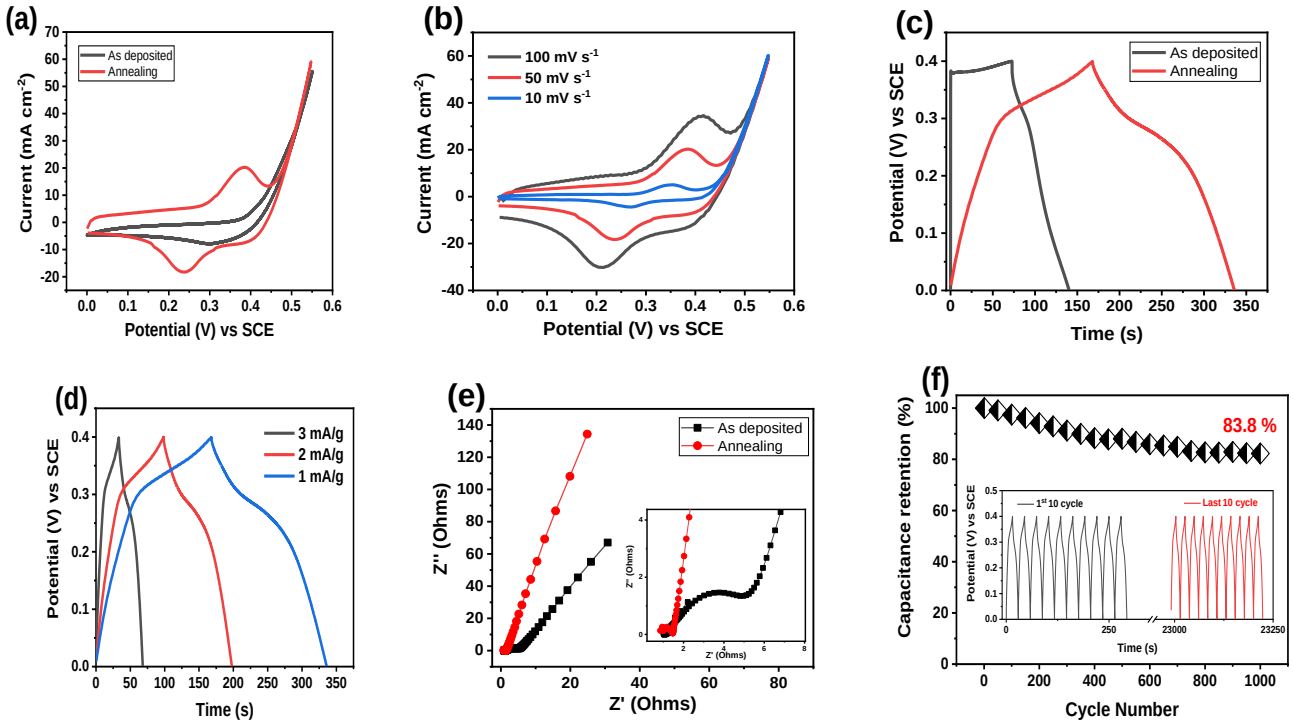

Fig. 4. (a) CV curve of as deposited and annealed NiS electrode (b) CV curves with various scan rates of annealed NiS electrode (c) GCD curve of as deposited and annealed NiS electrode (d) GCD curves with various current density of annealed NiS electrode (e) Nyquist plot of annealed NiS electrode (Inset shows high frequency region) (f) Capacity retention with GCD cyclic performance of NiS electrode for 1000 cycles (Inset shows first 10 and last 10 GCD cycles).

3. **Optical studies:**

The absorption spectrum of as-deposited and annealed films deposited on glass substrates was studied over visible range 350–850 nm. Fig2(a) shows the optical absorption of the as deposited and annealed films, it observes that, after annealing the absorption coefficient of films increases, similar results was found by reported by Jeon *et al.* [25] and Kulkarni *et al.* [26]. The optical band gap (Eg) for as prepared and annealed films is determined by the equation based on optical absorption spectra [27],

$$\alpha = \frac{A(Eg-h\nu)^n}{h\nu} \qquad (8)$$

where 'α' is the absorption coefficient, 'A' is a constant, 'Eg' is the band gap, hν is the photon energy, and 'n' is a constant number equal to 1/2 for direct gap and 2 for indirect gap compound. The plots of $(\alpha h\nu)^2$ versus hν of as deposited and annealed films are shown in Fig2(b). The band gaps are shown by extrapolating curves to the photon energy axis. Optical band gap decreases after annealing from 2.67 to 2.36 eV reveals, red shift as well as improved in crystallinity of sample.

4. Surface Morphology study:

The surface morphology of as-prepared and annealed NiS was investigated by Field Emission scanning electron microscopy (FESEM) Fig.3 (a) showed FESEM image of as-deposited thin films indicates the film surface looks accumulation of flakes and some overgrowth clusters. However, Fig.3 (b) revealed surface morphology of annealed sample. After annealing It was observed that, the formation of identical micro flakes' structure, which resulted into increase in porosity. Further the benefit of large surface area in the form of active sites gives high energy storage abilities. Such a flakes like microstructural surface with absence of agglomerations causes leads to a high performance of electrochemical activities. A histogram used to calculate the average flake's length of annealed NiS shown in fig 3 (c) indicated that average flake's length is 0.51 µm.

5. Electrochemical Investigation :

Electrochemical experiments were performed in a three-electrode electrochemical cell with NiS as a working electrode, platinum as a counter, and a saturated calomel electrode (SCE) as the reference electrode to investigate their performance as a positive electrode material for supercapacitors in aqueous 1M KOH electrolyte. The electrochemical performance of both samples was tested by CV, GCD, EIS, and cyclic stability as shown in Fig4.

Fig.4 (a). showed a comparison of typical CV curves at scan rate of 50 mVs^{-1} in a potential window of 0.0 to 0.55 V. It is observed that the significant oxidation and reduction peaks values of annealed electrode with respect to as deposited electrode resulted into more area under the CV curve, implying that annealed electrode has high capability of charge store. Fig.4 **(b).** represents the CV curves of annealed NiS electrodes at different scan rates (10, 50, and 100 mV s^{-1}) in 1 M KOH electrolyte. The CV curves show a redox peak, indicating that electrochemical charge storage is due to the redox reaction of the NiS electrode. The CV curves exhibit a variety of oxidation and reduction peaks with reversible charge transfer. The redox peak intensity of CV curves increases as the scan rate increases. The position of the redox peak is migrating slightly towards positive and negative potentials, this is caused by the polarization of lower electrical conductivity in free electrons of NiS electrode [28]. In general, electron charge transfer in reversible electrochemical processes was accomplished via an OH^- ion disturbed form of the Ni^{2+} / Ni^{3+} redox pair [29]. The annealed NiS electrodes showed very strong redox peaks due to the following Faradaic reactions 9 and 10.

$$NiS + OH^- \leftrightarrow NiSOH + e^- \quad (9)$$

$$NiSOH + OH^- \leftrightarrow NiSO + H_2O + e^- \quad (10)$$

Furthermore, the current response of the oxidation peak rises as the scan rate increases from 10-100 mV s^{-1}, indicating that the NiS electrode contains a greater number of electroactive sites. The greater current response shown by annealed NiS electrode gives better specific capacitance (C_s), the C_s of both electrodes are calculated from CV and GCD values by following equation 11 & 12,

$$C_s = \frac{\int I\,dv}{m.v.\Delta V} \quad (11)$$

$$C_s = \frac{I\Delta t}{m.\Delta V} \quad (12)$$

Where, $\int I\,dv$ is integral area under the CV curve, (m) is mass of sample, (v) is scan rate, & (ΔV) is voltage window, (I) is the discharge current, (Δt) is the discharge time of electrode. The C_s exhibited from eq. (11) of annealed and as deposited electrode are 637 F g^{-1} & 151Fg^{-1} at 50 mVs^{-1}. The annealed NiS electrode showed maximum C_s , due to the flakes-like microstructure surface. The C_s values are 655 Fg^{-1}, 637 Fg^{-1}, and 592 Fg^{-1} at 10, 50 and 100 mV s^{-1} scan

rate respectively. The annealed NiS electrode have more electroactive sites than as deposited electrode in electrochemical reactions, consequently C_s improves.

Fig.4 (c) shows, the annealed and as deposited electrode's charge storage capabilities by the galvanostatic charge discharge (GCD) curves at 1 $mAcm^{-2}$ constant current density. The non-linearity of the GCD curves is distinct from the general linear discharge characteristic of non-faradic charge storage mechanism, as determined by the above CV test. The annealed NiS electrode exhibits an extended discharge curve that is similar to the CV data. From the eq. (12) at 1 $mAcm^{-2}$ of constant current density the calculated specific capacitances, for the as deposited and annealed electrodes are found to be 140 $Fg^{-1}$and 641 Fg^{-1} respectively. Furthermore, the supercapacitive behaviour of the annealed NiS electrode at various current densities (1 to 3 mA cm^{-2}) as shown in Fig.4 (d). The discharge time decreases as the current density increases; this linearity indicates good electrochemical performance. For annealed NiS electrode the C_s values are 641 Fg^{-1}, 601 Fg^{-1}, and 575 Fg^{-1} at 1, 2 and 3$mAcm^{-2}$ current density respectively. The annealed NiS electroactive material features an abundant active site that allows high storage of energy through its larger surface area and specific capacitance than earlier reports [10-14].

As shown in fig.4 (e) electrochemical impedance spectra (EIS) measurements for both electrodes were carried out at open circuit potential (OCP) over the frequency range of 10 MHz to 0.01 Hz. where Z' and Z" are the real and imaginary impedance portions. The high and low frequency portions are related to the semicircle and straight line of impedance spectra respectively explored in fig inset [30]. The annealed NiS electrode exhibits vertical sloping straight line at the low frequency region and smaller depressed arc at high frequency region indicates lower charge transfer resistance (R_{ct}) and lower Polarization resistance (R_p) values. The lower R_{ct} is observed for annealed electrode 0.74 Ω cm^{-2}. However, as deposited NiS electrode showed significantly higher value of 3.85 Ωcm^{-2}. Similarly, R_p values for as deposited and annealed electrode are found to be 0.96 and 0.85 Ωcm^{-2} respectively. The flakes-like microstructure of annealed NiS electrode with high crystallinity via annealing process, leads to enhance active sites and assisting in the reduction of R_{ct} and R_p values and this is in good agreement with band gap effect associated with our samples. Fig.4 (f) showed the electrochemical GCD cyclic stabilities of annealed NiS electrode for 1000 charge discharge cycles. The inset graphic represents the first and last ten cycles of the GCD curve. It is noting that the specific capacitance slowly decreased to 83.8% of the initial capacitance up to 1000 cycles, demonstrating a good electrochemical stability.

Conclusion

In conclusion, stainless steel supported flakes like hexagonal NiS thin film electrodes were successfully synthesized by simple and low-cost CBD approach. The effect of the annealing process caused an amorphous to polycrystalline transformation of electrode with improved structural, optical and electrochemical properties of nickel sulphide electrode. The porous and flakes like morphology of NiS electrode generate the high electroactive sites with increase in faradaic redox activity on electrode surface and provide short path for electrolyte ion transfer. The optical studies showed direct band gap of 2.36 eV with lower charge transfer and polarization resistance values for efficient and easy electrochemical paths in storage mechanism. Annealed Nickle sulphide electrode showed specific capacitance of 655 Fg^{-1} at 10 mVs^{-1} scan rate and 641 Fg^{-1} at 1.0 mAg^{-1} current density in aqueous 1M KOH electrolyte with retaining ~83% stability after 1000 cycles. Thus, NiS electrode is strong contender for supercapacitor application by cost effective simple chemical route.

Acknowledgement: Authors are very much grateful to the Science & Engineering Research Board (SERB), New Delhi under for financial support through the scheme no ECR/2017/002820.

Conflicts of interest: The authors stated that no conflicts of interest.

References

1. Elmorshedy, M. F., Elkadeem, M. R., Kotb, K. M., Taha, I. B. M., & Mazzeo, D. (2021). Optimal design and energy management of an isolated fully renewable energy system integrating batteries and supercapacitors. Energy Conversion and Management, 245, 114584. doi:10.1016/j.enconman.2021.114584 10.1016/j.enconman.2021.114584.
2. Wang, Y., Zhang, L., Hou, H., Xu, W., Duan, G., He, S., Jiang, S. (2020). Recent progress in carbon-based materials for supercapacitor electrodes: a review. Journal of Materials Science. doi:10.1007/s10853-020-05157-6 10.1007/s10853-020-05157-6.
3. Erdem, E., & Najib, S. (2019). Current progress achieved in novel materials for supercapacitor electrodes: Mini Review. Nanoscale Advances. doi:10.1039/c9na00345b 10.1039/c9na00345b
4. Wang, D.-G., Liang, Z., Gao, S., Qu, C., & Zou, R. (2020). Metal-organic framework-based materials for hybrid supercapacitor application. Coordination Chemistry Reviews, 404, 213093. doi:10.1016/j.ccr.2019.213093 10.1016/j.ccr.2019.213093
5. Theerthagiri, J., Senthil, R. A., Nithyadharseni, P., Lee, S. J., Durai, G., Kuppusami, P., Choi, M. Y. (2020). Recent progress and emerging challenges of transition metal sulfides based composite electrodes for electrochemical supercapacitive energy storage. Ceramics International. doi:10.1016/j.ceramint.2020.02.270 10.1016/j.ceramint.2020.02.270
6. Das, A., Raj, B., Mohapatra, M., Andersen, S. M., & Basu, S. (2021). Performance and future directions of transition metal sulfide-based electrode materials towards supercapacitor / supercapattery. WIREs Energy and Environment. doi:10.1002/wene.41410.1002/wene.414
7. Pothu, R., Bolagam, R., Wang, Q.-H., Ni, W., Cai, J.-F., Peng, X.-X., Ma, J.-M. (2020). Nickel sulfide-based energy storage materials for high-performance electrochemical capacitors. Rare Metals. doi:10.1007/s12598-020-01470-w 10.1007/s12598-020-01470-w
8. Sarker, J. C., & Hogarth, G. (2021). Dithiocarbamate Complexes as Single Source Precursors to Nanoscale Binary, Ternary and Quaternary Metal Sulfides. Chemical Reviews, 121(10), 6057–123. doi:10.1021/acs.chemrev.0c01183 10.1021/acs.chemrev.0c01183
9. Li, B., Zheng, M., Xue, H., & Pang, H. (2016). High performance electrochemical capacitor materials focusing on nickel based materials. Inorganic Chemistry Frontiers, 3(2), 175–202. doi:10.1039/c5qi00187k 10.1039/c5qi00187k
10. Zhu, T., Wu, H. B., Wang, Y., Xu, R., & Lou, X. W. D. (2012). Formation of 1D Hierarchical Structures Composed of Ni3S2Nanosheets on CNTs Backbone for Supercapacitors and Photocatalytic H2Production. Advanced Energy Materials, 2(12), 1497–1502. doi:10.1002/aenm.201200269 10.1002/aenm.201200269
11. Yang, J., Duan, X., Qin, Q., & Zheng, W. (2013). Solvothermal synthesis of hierarchical flower-like β-NiS with excellent electrochemical performance for supercapacitors. Journal of Materials Chemistry A, 1(27), 7880. doi:10.1039/c3ta11167a 10.1039/c3ta11167a
12. Patil, A. M., Lokhande, A. C., Chodankar, N. R., Kumbhar, V. S., & Lokhande, C. D. (2016). Engineered morphologies of β -NiS thin films via anionic exchange process and their supercapacitive performance. Materials & Design, 97, 407–416. doi:10.1016/j.matdes.2016.02.114 10.1016/j.matdes.2016.02.114
13. S., N., A., J. C. M., & G., M. (2018). Facile microwave-hydrothermal synthesis of NiS nanostructures for supercapacitor applications. Applied Surface Science, 449, 485–491. doi:10.1016/j.apsusc.2018.01.024 10.1016/j.apsusc.2018.01.024
14. Yu, L., Yang, B., Liu, Q., Liu, J., Wang, X., Song, D., Jing, X. (2015). Interconnected NiS nanosheets supported by nickel foam: Soaking fabrication and supercapacitors application. Journal of Electroanalytical Chemistry, 739, 156–163. doi:10.1016/j.jelechem.2014.12.031 10.1016/j.jelechem.2014.12.031
15. Mane, R. S., & Lokhande, C. D. (2000). Chemical deposition method for metal chalcogenide thin films. Materials Chemistry and Physics, 65(1), 1–31. doi:10.1016/s0254-0584(00)00217-0 10.1016/s0254-0584(00)00217-0
16. Pawar, S. M., Pawar, B. S., Kim, J. H., Joo, O.-S., & Lokhande, C. D. (2011). Recent status of chemical bath deposited metal chalcogenide and metal oxide thin films. Current Applied Physics, 11(2), 117–161. doi:10.1016/j.cap.2010.07.007 10.1016/j.cap.2010.07.007
17. Patil, U. M., Kulkarni, S. B., Jamadade, V. S., & Lokhande, C. D. (2011). Chemically synthesized hydrous RuO2 thin films for supercapacitor application. Journal of Alloys and Compounds, 509(5), 1677–1682. doi:10.1016/j.jallcom.2010.09.133 10.1016/j.jallcom.2010.09.133.
18. Patil, U. M., Lee, S. C., Sohn, J. S., Kulkarni, S. B., Gurav, K. V., Kim, J. H., Jun, S. C. (2014). Enhanced Symmetric Supercapacitive Performance of Co(OH)2 Nanorods Decorated Conducting Porous Graphene Foam Electrodes. Electrochimica Acta, 129, 334–342. doi:10.1016/j.electacta.2014.02.063 10.1016/j.electacta.2014.02.063.

19. Pan, Y., Chen, Y., Li, X., Liu, Y., & Liu, C. (2015). Nanostructured nickel sulfides: phase evolution, characterization and electrocatalytic properties for the hydrogen evolution reaction. RSC Advances, 5(127), 104740–104749. doi:10.1039/c5ra18737k 10.1039/c5ra18737k

20. Hübener, S. (2003). Actinide Elements. Encyclopedia of Physical Science and Technology, 211–236. doi:10.1016/b0-12-227410-5/00011-9 10.1016/b0-12-227410-5/00011-9

21. Holzwarth, U., & Gibson, N. (2011). The Scherrer equation versus the "Debye-Scherrer equation." Nature Nanotechnology, 6(9), 534–534. doi:10.1038/nnano.2011.145 10.1038/nnano.2011.145

22. Louër, D. (2017). Powder X-Ray Diffraction, Applications. Encyclopedia of Spectroscopy and Spectrometry, 723–731. doi:10.1016/b978-0-12-803224-4.00257-0 10.1016/b978-0-12-803224-4.00257-0

23. Feijoo, I., Cabeza, M., Merino, P., Pena, G., Pérez, M. C., Cruz, S., & Rey, P. (2018). Estimation of crystallite size and lattice strain in nano-sized TiC particle-reinforced 6005A aluminium alloy from X-ray diffraction line broadening. Powder Technology. doi:10.1016/j.powtec.2018.11.010 10.1016/j.powtec.2018.11.010

24. Khalate, S. A., Kate, R. S., Pathan, H. M., & Deokate, R. J. (2017). Structural and electrochemical properties of spray deposited molybdenum trioxide (α-MoO3) thin films. Journal of Solid State Electrochemistry, 21(9), 2737–2746. doi:10.1007/s10008-017-3540-4 10.1007/s10008-017-3540-4

25. Jeon, J.-W., Jeon, D.-W., Sahoo, T., Kim, M., Baek, J.-H., Hoffman, J. L., Lee, I.-H. (2011). Effect of annealing temperature on optical band-gap of amorphous indium zinc oxide film. Journal of Alloys and Compounds, 509(41), 10062–10065. doi:10.1016/j.jallcom.2011.08.033 10.1016/j.jallcom.2011.08.033

26. Kulkarni, S. B., Patil, U. M., Salunkhe, R. R., Joshi, S. S., & Lokhande, C. D. (2011). Temperature impact on morphological evolution of ZnO and its consequent effect on physico-chemical properties. Journal of Alloys and Compounds, 509(8), 3486–3492. doi:10.1016/j.jallcom.2010.12.036 10.1016/j.jallcom.2010.12.036

27. Kokilavani, S., Al-Kheraif, A. A., Thomas, A. M., Syed, A., Elgorban, A. M., Raju, L. L., Khan, S. S. (2021). Novel NiS/Ag2MoO4 heterostructure nanocomposite: Synthesis, characterization and superior antibacterial and enhanced photocatalytic activity. Physica E: Low-Dimensional Systems and Nanostructures, 133, 114767. doi:10.1016/j.physe.2021.114767 10.1016/j.physe.2021.114767

28. Elgrishi, N., Rountree, K. J., McCarthy, B. D., Rountree, E. S., Eisenhart, T. T., & Dempsey, J. L. (2017). A Practical Beginner's Guide to Cyclic Voltammetry. Journal of Chemical Education, 95(2), 197–206. doi:10.1021/acs.jchemed.7b00361 10.1021/acs.jchemed.7b00361

29. Chen, H., Wu, Z., Zhong, Y., Chen, T., Liu, X., Qu, J., Zhong, B. (2019). Boosting the reactivity of Ni2+/Ni3+ redox couple via fluorine doping of high performance Na0.6Mn0.95Ni0.05O2-F cathode. Electrochimica Acta. doi:10.1016/j.electacta.2019.04.003 10.1016/j.electacta.2019.04.003

30. Wang, S., Zhang, J., Gharbi, O., Vivier, V., Gao, M., & Orazem, M. E. (2021). Electrochemical impedance spectroscopy. Nature Reviews Methods Primers, 1(1). doi:10.1038/s43586-021-00039-w 10.1038/s43586-021-00039-w